

# Structure and aggregation of colloids immersed in critical solvents

T. F. Mohry,<sup>1,2, a)</sup> A. Maciolek,<sup>1,2,3, b)</sup> and S. Dietrich<sup>1,2, c)</sup>

<sup>1)</sup>Max-Planck-Institut für Intelligente Systeme, Heisenbergstraße 3, 70569 Stuttgart, Germany

<sup>2)</sup>Universität Stuttgart, Institut für Theoretische und Angewandte Physik, Pfaffenwaldring 57, 70569 Stuttgart, Germany

<sup>3)</sup>Institute of Physical Chemistry, Polish Academy of Sciences, Kasprzaka 44/52, PL-01-224 Warsaw, Poland

(Dated: 28 October 2018)

We consider an ensemble of spherical colloidal particles immersed in a near-critical solvent such as a binary liquid mixture close to its critical demixing point. The emerging long-ranged fluctuations of the corresponding order parameter of the solvent drive the divergence of the correlation length. Spatial confinements of these critical fluctuations by colloidal solute particles, acting as cavities in the fluctuating medium, restrict and modify the fluctuation spectrum in a way which depends on their relative configuration. This results in effective, so-called critical Casimir forces (CCFs) acting on the confining surfaces. Using the available knowledge about CCFs we study the structure and stability of such colloidal suspensions by employing an approach in terms of effective, *one*-component colloidal systems. Applying the approximation of pairwise additive CCFs we calculate the radial distribution function of the colloids, which is experimentally accessible. We analyze colloidal aggregation due to CCFs and thus allude to previous experimental studies which are still under debate.

PACS numbers: 61.20.Gy, 64.60.fd, 64.70.pv, 64.75.Xc, 82.70.Dd

## I. INTRODUCTION

In colloidal suspensions with near-critical solvents, colloidal particles acting as cavities impose boundary conditions at the colloid surfaces for the fluctuating order-parameter (OP) of the solvent and perturb the OP field on the length scale of the bulk correlation length  $\xi(t = (T - T_c^{(s)})/T_c^{(s)} \rightarrow 0) \sim |t|^{-\nu}$ , which diverges upon approaching the bulk critical temperature  $T_c^{(s)}$  of the solvent;<sup>1</sup>  $\nu$  is a standard critical bulk exponent. These modifications of the OP and the restrictions of its fluctuation spectrum result in an effective force acting between the colloids, known as the so-called critical Casimir force (CCF).<sup>1</sup> For equal boundary conditions, i.e., equal preference of all colloids for one of the two species of the binary solvent, the CCF is attractive and can lead to reversible aggregation phenomena. Aggregation phenomena are of considerable interest due to their relevance for the stability of colloidal suspensions.

In our preceding paper<sup>2</sup> we have investigated the phase behavior of colloidal suspensions with near-critical solvents and have explored the possibility of a phase separation into two thermodynamic phases, one being rich and the other being poor in colloidal particles. If the effective attraction potential between colloidal particles is sufficiently strong, a condensation of colloids into a stable *equilibrium* liquid phase may be preempted (on the time scale of observation) by the formation of *non-equilibrium*

aggregates in which the colloidal particles stick together. In general, these aggregates may grow and shrink and their structure depends on the packing fraction of the colloidal particles in the aggregates and on the strength of the attraction among the colloidal particles. In general the aggregates may consist of crystalline structures, gels, glasses, but also loose fractal aggregates may occur. In the present paper we shall address the possibility of aggregation of colloids immersed in near-critical binary liquid mixtures serving as their solvent.

Beysens and Estève<sup>3</sup> have reported aggregation phenomena for silica spheres immersed in a binary liquid mixture of water and lutidine which exhibits a miscibility gap with a lower critical point.<sup>4,5</sup> Using light scattering these authors found that upon approaching the bulk coexistence region of demixing from the one-phase region of the binary liquid mixture at constant composition of the solvent, the silica spheres coagulate reversibly at rather well defined temperatures. Moving back the thermodynamic state deeply into the one-phase region the coagulated aggregates dissolve again. These observations, i.e., the formation of colloidal aggregates which sediment, have been confirmed later for silica and polystyrene particles immersed in the same solvent<sup>6-11</sup> and have been reported also for other systems;<sup>9,11-16</sup> for reviews see Ref. 17. The experimental findings have been interpreted as (the precursors of) a phase transition in the ternary mixture<sup>11-13</sup> or as a (non-equilibrium) coagulation, which can be caused by various mechanisms. Some aspects of these experimental observations will be discussed in more detail in Sect. VI.

Generically, colloidal particles have a preference for one of the two components of the binary solvent. At the surface of the colloid this preference gives rise to a surface

<sup>a)</sup>Electronic mail: mohry@is.mpg.de

<sup>b)</sup>Electronic mail: maciolek@is.mpg.de

<sup>c)</sup>Electronic mail: dietrich@is.mpg.de

field conjugate to the order parameter at the surface and thus leads to an adsorption layer rich in this component. Upon approaching the critical point along the two-phase coexistence curve, at the wetting transition the adsorption layers on the surface of the spherical colloids become thick (but stay finite) so that they can snap if the colloids get sufficiently close.<sup>18</sup> This leads to attractive interactions<sup>18</sup> and can give rise to coagulation.

Close to the critical point CCFs provide an additional mechanism for mutual attraction between the colloids. Experimentally it has been observed that (strong) coagulation occurs for compositions of the solvent for which the concentration  $c_a$  of the adsorbed component preferred by the colloids is comparable but less than its value at the critical point, i.e., when  $c_a \lesssim c_{a,c}^{(s)}$ . This observation is in line with both explanations mentioned above because the wetting transition is indeed located in that region of the bulk phase diagram of the solvent and because the CCFs are stronger there<sup>19</sup> than for  $c_a \gtrsim c_{a,c}^{(s)}$ . Several theoretical approaches have been used in order to study this aggregation phenomenon for colloids immersed in a solvent which is close to its phase separation.<sup>20–24</sup> Most of them, however, stay on a qualitative level of description, pointing out the possibility of coagulation.

Here we present a *quantitative* analysis of the stability of monodisperse spherical colloidal particles immersed in a critical binary solvent. Our analysis is based on controlled approximations which we have worked out in Ref. 2. Following Ref. 2 we adopt a description in terms of an effective one-component system. Within this approach the presence of the solvent is taken into account via an effective pair potential of the colloids. For the regular background interaction potential we consider a generic, softly repulsive contribution. The CCFs depend on the configuration of all colloidal particles and thus are in general non-additive. We focus on dilute suspensions with low colloidal number density  $\rho$ , for which the approximation of pairwise additive CCFs is valid. The critical Casimir pair potential between two spherical particles immersed in a binary liquid mixture is described in terms of a universal scaling function corresponding to the Ising universality class with symmetry-breaking boundary conditions.<sup>19,25–30</sup> We apply the Derjaguin approximation, within which the pair potential between two spheres is expressed in terms of the scaling function of the CCF in a slab.<sup>30–32</sup> The Derjaguin approximation

can be applied, if the surface-to-surface distances  $D$  between the objects on which the CCF acts, i.e.,  $D \lesssim \xi$ , are small compared with the radius  $R$  of the colloids.

In  $d = 3$  and for a vanishing bulk ordering field  $h_b = 0$ , the corresponding scaling function is known from Monte Carlo simulations,<sup>33–36</sup> from field-theoretical studies,<sup>37</sup> and from the extended de Gennes–Fisher local-functional method.<sup>38,39</sup> Corresponding experimental data<sup>32,40–42</sup> are also available. The conjugate ordering field  $h_b$  of the order parameter of the solvent corresponds to the chemical potential difference of the two species forming the binary liquid mixture. The reversible aggregation phenomenon of colloids is observed for thermodynamic states of the solvent which correspond to a nonzero  $h_b$ . In order to handle the dependence of the CCF on this ordering field within the Derjaguin approximation, we use still another approximation for the film scaling function of the CCF in  $d = 3$  (see, c.f., Eq. (3)). The scaling functions resulting from this approximation are comparable with the ones obtained using the extended de Gennes–Fisher local-functional method<sup>43</sup> and are in qualitative agreement with corresponding curves provided in Ref. 16 which are based on a density functional approach.

Our presentation is organized as follows. In Sect. II we shortly summarize the effective one-component description which we use for our analysis. For more details and a comprehensive discussion of the validity and of the limitations of this description we refer to the preceding paper.<sup>2</sup> In Sect. III we discuss the possible functional forms of the effective interaction potential employed in our study. Section IV is concerned with aggregation phenomena in colloidal suspensions and in Sect. V results for the radial distribution function of the colloids are presented. In Sect. VI we compare available experimental data with our results. We summarize our study in Sect. VII.

## II. EFFECTIVE INTERACTIONS

We aim for a theoretical description of the behavior of monodisperse colloids immersed in a near-critical solvent. To this end we consider a monodisperse, effective one-component system of colloids with radius  $R$  for which the presence of the solvent enters via the following effective pair potential  $V(r = D + 2R)/(k_B T) = U(r = D + 2R)$ :

$$U(r) = \begin{cases} \infty, & D < 0 \\ U_{rep} + U_c^{(d=3)} = A \exp(-\kappa D) + (1/\Delta)\theta^{(d=3)}(\Theta, \Delta, \Sigma), & D > 0. \end{cases} \quad (1)$$

In Eq. (1) the background interaction potential between the colloids, which is present also away from  $T_c^{(s)}$ , consists of a hard core repulsion for center-to-center distances

$r < 2R$  and a soft, repulsive tail  $U_{rep}$  for  $D = r - 2R > 0$ . The latter prevents aggregation due to omnipresent effectively attractive dispersion forces. In the case of electro-

static repulsion, the range  $\kappa^{-1}$  of the repulsion is associated with the Debye screening length and its strength  $A$  depends on the colloidal surface charge density.<sup>44,45</sup> We do not consider an additional interaction which would account for effectively attractive dispersion forces. Effectively, dispersion forces can be switched off by using index-matched colloidal suspensions. As will be discussed in the next section, the presence of attractive dispersion forces does not change the conclusions of the present study. The critical Casimir potential  $U_c^{(d=3)}$  has a scaling form with  $\theta^{(d=3)}$  as its universal scaling function.  $\theta^{(d)}$  depends on the spatial dimension  $d$  and on the scaling variables  $\Theta = \text{sgn}(t) D/\xi$ ,  $\Delta = D/R$ , and  $\Sigma = \text{sgn}(h_b) \xi/\xi^{(h)}$ . The bulk correlation lengths  $\xi(t \geq 0) = \xi_0^\pm |t|^{-\nu}$  and  $\xi^{(h)} = \xi_0^{(h)} |h_b|^{-\nu/(\beta\delta)}$  govern the exponential decay of the bulk solvent OP correlation function for  $t \rightarrow 0^\pm$  at  $h_b = 0$  and for  $h_b \rightarrow 0$  at  $t = 0$ , respectively; one has  $t = (T_c^{(s)} - T)/T_c^{(s)}$  for a lower critical point. The amplitudes  $\xi_0^{\pm, h}$  are non-universal but related via universal amplitude ratios;  $\nu$ ,  $\beta$ , and  $\delta$  are standard bulk critical exponents.<sup>46</sup>

For  $\theta^{(d=3)}$  we use the Derjaguin approximation. For the configuration of two spheres it renders<sup>30-32</sup>

$$\theta_{Derj}^{(d=3)}(\Delta, \Theta, \Sigma) = \pi \int_1^\infty (x^{-2} - x^{-3}) \vartheta_{\parallel}^{(d=3)}(x\Theta, \Sigma) dx; \quad (2)$$

$\vartheta_{\parallel}^{(d)}(y, \Sigma)$  is the universal scaling function of the CCF  $f_{C,\parallel}$  per  $k_B T_c^{(s)}$  and per area  $A$  for a slab of the thickness  $L$ :  $f_{C,\parallel}/A = k_B T_c^{(s)} L^{-d} \vartheta_{\parallel}^{(d)}(y = \text{sgn}(t) L/\xi, \Sigma)$ . From Eq. (2) it follows that the scaling function  $\theta_{Derj}^{(d=3)}$  does not depend on  $\Delta$ , which therefore enters into Eq. (1) only as a prefactor. In the cases in which  $\Sigma = 0$ , i.e., for a vanishing bulk field  $h_b$  we use  $\vartheta_{\parallel}^{(3)}(y, \Sigma = 0)$  as determined from Monte Carlo simulations.<sup>33-36</sup>

The scaling function for nonzero  $\Sigma$  is obtained from the following approximation (see Eq. (24) in Ref. 2 and the subsequent discussion there):

$$\vartheta_{\parallel}^{(d)}(y, \Sigma) \simeq \vartheta_{\parallel}^{(d)}(y, \Sigma = 0) \frac{\vartheta_{\parallel}^{(d=4)}(y, \Sigma)}{\vartheta_{\parallel}^{(d=4)}(y, \Sigma = 0)}. \quad (3)$$

Within this approximation, for  $h_b \rightarrow 0$  the scaling function reduces exactly to  $\vartheta_{\parallel}^{(d)}(\Sigma = 0)$  (for all  $d$ ) and for fixed values of  $y$  its functional form is the one obtained from mean-field theory (MFT,  $d = 4$ ). The necessary input for this approximation is the mean-field scaling function of the CCF for the film geometry, which follows from the field-theoretical approach within the framework of the Landau-Ginzburg theory. For colloids strongly preferring one and the same of the two species of the binary liquid mixture the so-called strong adsorption limit applies. Accordingly, the appropriate boundary conditions are the ones breaking the symmetry of the OP at the colloid surfaces. We determine the CCF from the local OP profile  $\phi_{MFT}$  within MFT via the so-called stress-tensor  $\mathcal{T}$ .<sup>47</sup> The CCF per area in a slab, which is confined along the  $z$ -direction, is given by the  $(z, z)$  component of the stress tensor,  $f_{C,\parallel}^{(MFT)}/A = k_B T_c^{(s)} \langle \mathcal{T}_{z,z}[\phi_{MFT}] - \mathcal{T}_{z,z}[\phi_{b,MFT}] \rangle$  (see Eqs. (20) and (25) in Ref. 2).

Our results will be expressed in terms of the parameters

$$\begin{aligned} s &= \kappa R, & a &= A/s, & \zeta &= \text{sgn}(t) \kappa \xi, \\ \text{and} & & x &= \kappa D = \kappa R - 2s. \end{aligned} \quad (4)$$

Within this parametrization the functional form of  $U$  is determined by  $a$ ,  $\zeta$ , and  $\Sigma$ , while  $s$  tunes the overall strength of the potential without affecting its shape:

$$U(r = D + 2R) = \begin{cases} \infty & x < 0 \\ s \left\{ a \exp(-x) + (1/x) \theta_{Derj}^{(d=3)}(x/\zeta, \Sigma) \right\} & x > 0. \end{cases} \quad (5)$$

The parameter  $\zeta$  can be varied experimentally by changing the temperature (via  $\xi$ ) or by adding salt to the solution (via  $\kappa$ ); it expresses the competition between the length scales of electrostatic repulsion and of the attractive CCF. The strength of repulsion is measured by  $a$ ; it is usually kept constant.  $\Sigma$  is determined by the thermodynamic state of the solvent. The ranges of the values of the parameters entering into the effective potential (Eq. (5)) and of the scaling variable  $\Sigma$ , which correspond to possible experimental realizations, are discussed in detail in Ref. 2. The divergence  $\sim x^{-1}$  in  $U(D = x/\kappa \rightarrow 0)$  (see Eq. (5)) is unphysical,<sup>2</sup> because the scaling form used for

$U_c^{(d)}$  applies only for distances large compared with microscopic length scales such as  $\xi_0^\pm$ . In order to circumvent this unphysical behavior we shall apply a linear extrapolation scheme for  $U(D \rightarrow 0)$  whenever this is necessary.

### III. SHAPES OF THE EFFECTIVE POTENTIAL

By varying the thermodynamic state of the solvent the range and the strength of the attractive CCFs are changed. This variable attraction combined with the repulsive background contribution results in a broad va-

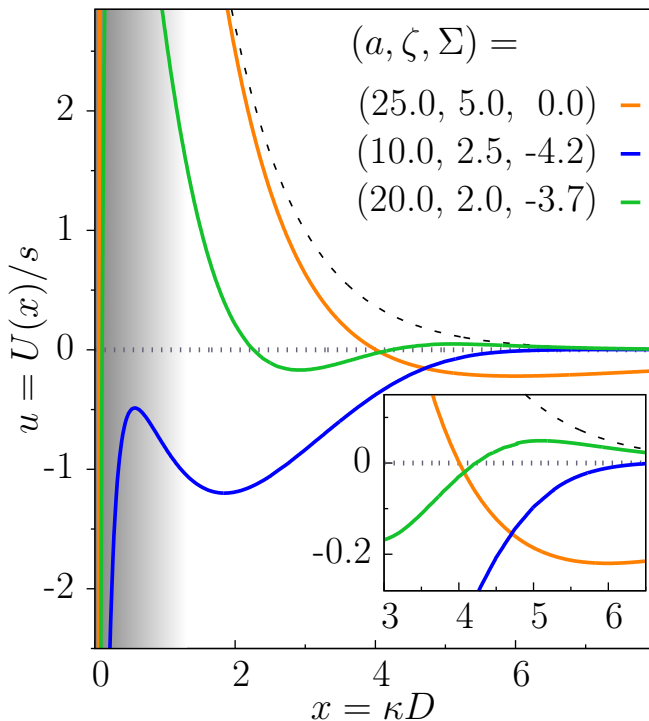


FIG. 1. Exemplary shapes of the effective pair potential given by Eq. (5). The dashed line represents the purely repulsive part of the potential for  $a = 20$ . The potentials considered here are physically appropriate for  $x = \kappa D \gtrsim 1$ . At smaller values of  $x$  (grayish area) additional (effective) forces can occur. In particular, the occurrence of a first minimum at contact, i.e., at  $D = 0$ , depends on microscopic details, which are not taken into account by Eq. (5).

riety of possible shapes of the effective potential given by Eq. (5). Examples of various shapes of this effective potential, as obtained for different values of the parameters  $a$ ,  $\zeta$ , and  $\Sigma$ , are shown in Fig. 1, where we plot the reduced potential  $u = U/s$  versus the reduced distance  $x = \kappa D$ . Depending on the values of the parameters, the CCFs compensate the repulsion for all values of  $D$  or only within certain regimes. Compensation for all values of  $D$  occurs if the strength  $a$  of the repulsion is not too strong. This is illustrated by the blue curve in Fig. 1 corresponding to the parameter values  $a = 10$ ,  $\zeta = 2.5$ , and  $\Sigma = -4.2$ . We recall that negative values of  $\Sigma$  correspond to solvent compositions which are poor in the species preferred by the colloids. For larger values of  $a$ , a secondary attractive minimum (i.e.,  $u < 0$ ) can occur (in addition to the primary global minimum for  $D \rightarrow 0$ , which will be discussed below), while for small distances  $D$  the potential maintains a repulsive part, as for the orange and green curves in Fig. 1. Since  $s = \kappa R$  can vary between ca. 10 and 100 a shallow minimum in  $u$  can correspond to a deep potential well in  $U$ . For suitably chosen parameters, such as for the green curve ( $a = 20$ ,  $\zeta = 2$ ,  $\Sigma = -3.7$ ) in Fig. 1, the potential may be repulsive at large distances  $D \rightarrow \infty$  and may have an attractive secondary minimum.

Thus the CCFs provide a mechanism for realizing short-ranged attractive and long-ranged repulsive interaction pair potentials as studied for example in Refs. 48 and 49 in related contexts. These studies have shown that such potentials give rise to complex phase behaviors of colloidal suspensions.

The issue of the contact value  $U(D = 0)$  and the possibility of the occurrence of a primary minimum at small values of  $D$  is subtle and, as pointed out in Sec. II, cannot be discussed in general in terms of the effective potential  $U$  given by Eq. (5). However,  $U$  captures the occurrence of the potential barrier for  $D \simeq \kappa^{-1}$  and its reduction due to the attractive CCFs which is sufficient for the focus of the present study, i.e., concerning the influence of the universal CCFs. The short-ranged interactions acting at distances  $D \ll \kappa^{-1}, \xi$  (with  $\xi \gg \xi_0$ ) depend sensitively on materials properties. But for the following reason they do not affect our consideration of the stability of colloidal suspensions. In the case of large  $a$ , the repulsion is strong enough such that the CCFs cannot significantly reduce the associated potential barrier. Therefore within experimental observation times only the pair-interaction potential  $U$  considered in Eq. (5) is relevant for determining the phase behavior and the coagulation process. The influence of attractive short-range forces could be observed only for very long waiting-times because the time scale for passing the barrier is  $\sim \exp(U)$  (see Subsect. IV below). On the other hand in the case of small  $a$  the CCFs fully compensate the repulsion. The estimates for the values of the parameters for which the repulsive barrier disappears and thus rapid coagulation sets in can be obtained from the effective potential  $U$  given in Eq. (5). However, in order to be able to determine the detailed process of coagulation a truly microscopic description is needed. This is beyond the scope of the present study devoted to *universal* features. As long as no additional microscopic forces compete with the considered effective potential, Eq. (5) provides a description which is sufficient for the present purpose.

#### IV. STABILITY

The stability of colloidal suspensions and the aggregation of colloids are related to kinetic processes (see Ref. 45 and references therein). They are based on the diffusion of single particles in the presence of other particles of the same kind, interacting with them via interaction potentials which contain both attractive and repulsive contributions. For interacting particles, which irreversibly stick together once their surfaces touch each other, Fuchs introduced, using Smulochowski's theory, the stability ratio  $W$ ,<sup>50</sup>

$$W = 2R \int_{2R}^{\infty} \frac{\exp\{U(r)\}}{r^2} dr. \quad (6)$$

For hard spheres  $W = 1$ , while for  $W > 1$  ( $W < 1$ ) the repulsive (attractive) part of the interaction potential  $U$

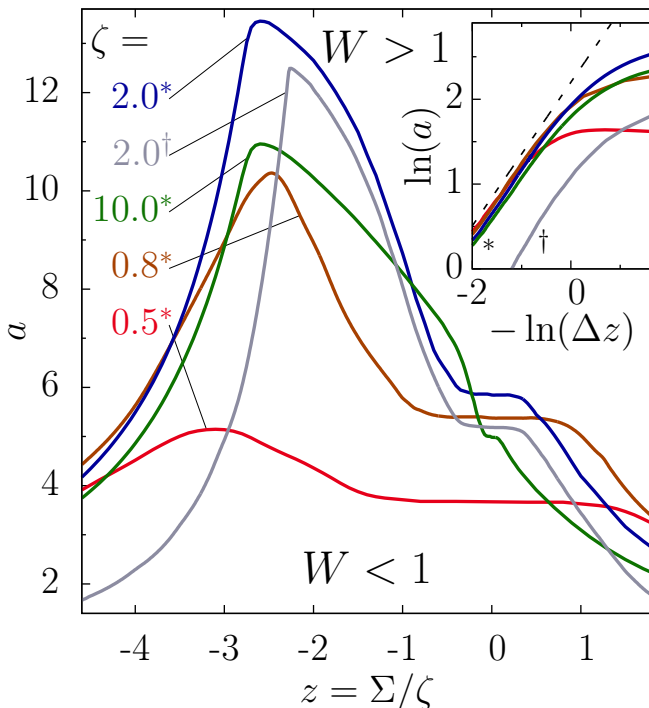


FIG. 2. Contour lines of constant stability ratio  $W = 1$  (Eq. (6)) for the effective pair potential given in Eq. (5) as function of  $a$  and  $\Sigma$  for various (fixed) values of  $\zeta$ . The star and the dagger superscripts correspond to  $s = 10$  and  $s = 50$ , respectively. For values  $W < 1$  (the region below the corresponding contour line) the colloids coagulate rapidly. For a binary solvent with compositions which are smaller, i.e., slightly poorer in the component preferred by the colloids, than the critical composition, i.e., for  $\Sigma \lesssim 0$ , this region ( $W < 1$ ) broadens towards larger values of the parameter  $a$  of the repulsion strength. The logarithmic plot in the inset shows, that for rather large negative values of  $\Sigma$  the contour lines decay according to a power law as function of  $\Delta z = z_m - z$ . The slope of the dashed line is 0.84;  $z_m = -2.6$  approximates the position of the maxima of the contour lines.

dominates. If there is a potential barrier, i.e.,  $U(r) \gg 1$  for a certain range of distances  $r > 2R$ , which leads to  $W > 1$ , on intermediate time scales the suspension will equilibrate into a (meta)stable homogeneous state. Only on very large time scales cluster formation sets in slowly. It turns out that  $W$  is proportional to the ratio between the characteristic times for diffusion of a single particle,  $t_{diff}$ , and for the formation of a pair of particles,  $t_{pair}$ :<sup>45</sup>

$$t_{diff}/t_{pair} = 3\eta/W, \quad (7)$$

with the packing fraction  $\eta = (4\pi/3)R^3\rho$ ;  $\rho$  is the number density of the colloidal particles.

We have calculated the stability ratio  $W = W(a, s, \zeta, \Sigma)$  according to Eq. (6) by using Eq. (5) within the one-phase region. Since the stability ratio  $W$  depends exponentially on the potential, in the calculation of  $W$  we can afford to omit the use of a cut-off at small distances  $D$ . The main contribution to  $W$  stems from the

maximum of the potential. The use of a cut-off would only slightly change the value of  $W$  but it would require an additional specification which is not necessary for this analysis.

In Fig. 2 the contour lines  $W = 1$  are plotted in the space spanned by the parameters  $a$  and  $z = \Sigma/\zeta$  for various values of  $\zeta$ . Changing  $\Sigma$  for fixed  $\zeta$  and  $s$  corresponds to moving along an isotherm in the thermodynamic space of the system. In order to have the contour lines on the same scale, it is useful to introduce the reduced variable  $\Sigma/\zeta$  as abscissa. For  $W = 1$  the time scales of diffusion and pairing of two particles are comparable (Eq. (7)). For a given value of  $\zeta$ , in the region  $W > 1$  above the corresponding contour line the suspension initially equilibrates into a (metastable) fluid state. If the potential has its global minimum at  $D = 0$ , e.g., due to van-der-Waals forces, aggregates may form eventually at long times; these time scales depend on the value of  $W$ . On the other hand, for  $W < 1$  rapid coagulation sets in.

The overall characteristics of the shape of contour lines  $W = 1$  remains the same for different (but fixed) values of  $\zeta$  and  $s$  (see Fig. 2). Upon decreasing  $\Sigma$  towards slightly negative values (i.e., for a binary solvent upon decreasing the amount of the component preferred by the colloids relative to the critical composition) the colloidal stability remarkably decreases, i.e., the contour line  $W = 1$  is shifted to larger values of the parameter  $a$  of the repulsion strength. For even more negative values of  $\Sigma$ , the system is driven far away from criticality, so that the attraction due to the CCFs weakens and stability is favored again. The position  $z_{max}$  of the maximum of the corresponding line  $a = a(z = \Sigma/\zeta)$  (given by  $W(a, s, \zeta, \Sigma = z\zeta) = 1$  for fixed  $s$  and fixed  $\zeta$ ) does hardly vary with  $\zeta$ . However the amplitude of  $a(z)$  and in particular the maximum value  $a_{max} = a(z_{max})$  exhibit a significantly nonmonotonous dependence on  $\zeta \sim |t|^{-\nu}$ . The value of  $a_{max}$  is largest for  $\zeta \simeq 2$ . This behavior reflects the fact that for  $(+, +)$  boundary conditions (i.e., equal surface fields on both surfaces) as considered here the CCFs are not strongest at  $T_c^{(s)}$  and  $h_b = 0$ , but slightly within the one-phase region and for small negative values of  $h_b$ .

The contour lines corresponding to a fixed value of  $s$  and various values of  $\zeta$  merge to a single curve for large negative and large positive values of  $\Sigma/\zeta$ . This behavior can be explained by the fact that for large values of  $|\Sigma|$  the scaling functions  $\theta_{Derj}^{(d=3)}$  ( $\Theta = D/\xi, \Sigma$ ) plotted as a function of  $\Theta\Sigma$  for various values of  $\Sigma$  fall onto each other.<sup>43</sup> Interestingly, within the plotted range of large negative values of  $z = \Sigma/\zeta$  the (common) decay of the contour lines can be described by a power law  $\sim (z_m - z)^{-p} = \Delta z^{-p}$  (see the double logarithmic plot in the inset of Fig. 2, where  $z_m = -2.6$  approximates the various  $z_{max}(\zeta)$  and  $p \simeq 0.84$ ). In the limit of strong bulk fields, i.e.,  $|h_b| \rightarrow \infty$ , the CCFs are vanishingly small. In this limit,  $W = 1$  for HS without a soft repulsive contribution and therefore  $(a(|z| \rightarrow \infty))_{W=1} \rightarrow 0$ . The leveling off of the contour lines  $W = 1$  close to  $\Sigma = 0$  is a

consequence of the choice of the abscissa  $\sim h_b^{\nu/(\delta\beta)}$ . As a function of  $h_b$  the contour lines exhibit no leveling off around  $z = 0$ .

The potential under consideration (within the Derjaguin approximation) is proportional to the parameter  $s$ . Thus with increasing (decreasing) values of  $s$  the region  $W < 1$  of aggregation shrinks (widens), because the repulsive barrier in  $U$  becomes larger (smaller). However, since the repulsive barrier contributes exponentially to  $W$ , the boundary of the region  $W < 1$  is mostly determined by the sheer occurrence of the repulsive barrier (which, however, is independent of  $s$ ) and therefore the dependence of the contour line  $W = 1$  on  $s$  is weak. This is seen in Fig. 2 where for  $\zeta = 2$  we compare the contour lines  $W = 1$  for  $s = 10$  and  $s = 50$  (the blue and gray curves, respectively). Note, that this weak dependence of the stability region on the parameter  $s = \kappa R$  is in contrast to the strong dependence on  $s$  of the two-phase region of the effective colloidal system, as discussed in Ref. 2 (see especially Fig. 3 therein). For the two-phase region not only the existence but also the actual strength of the attraction is important, and therefore it is sensitive to the value of  $s$ , because  $U \sim s$ .

The contour lines in Fig. 2 of constant stability ratio  $W = 1$  can be compared with the contour lines in Fig. 3 in Ref. 2 of constant critical temperature  $T_c^{(eff)}$  (or  $\zeta_c^{(eff)}$ ) delimitating the "liquid"- "gas" coexistence of the effective one-component colloidal system. In both figures the contour lines are plotted in the plane spanned by the parameter  $a$ , measuring the strength of the repulsion of the effective pair potential, and the scaling variable  $\Sigma$  (or  $\Sigma$  rescaled by the fixed value of  $\zeta$ ). The gross features of these contour lines are similar but the values of  $a$  are rather different. (Note the different scales for  $a$  in these two figures.) For example, for the same value of  $s = \kappa R = 10$ , at the temperature corresponding to  $\zeta = 2$  strong coagulation (i.e.,  $W < 1$ ) occurs for  $a \lesssim 13$ , whereas at the comparable temperature corresponding to  $\zeta = 3$  the colloidal suspension starts to phase separate already for a much stronger repulsion, i.e., for  $a \lesssim 300$  (see the blue curves in Fig. 3 in Ref. 2). We note, however, that phase separation occurs at relatively high packing fractions  $\eta \gtrsim 0.06$  of the colloidal particles (see also Subsect. III B in Ref. 2) whereas aggregation occurs also for very small packing fractions of the colloidal particles.

The experimentally relevant case of the variation of the stability ratio  $W$  with temperature at constant OP is shown in a semi-logarithmic plot in Fig. 3 in terms of  $\zeta \sim |t|^{-\nu}$  and the parameter  $m_0$  which is related to the OP; for  $t > 0$  it is given by (see Eq. (27) in Ref. 2)

$$m_0 = \text{sgn}(\phi) (\zeta_0^+)^{1/\nu} |\mathcal{B}/\phi|^{1/\beta} \quad (8)$$

and  $\zeta_0^+ = \kappa \xi_0^+$ .

$\phi$  and  $h_b$  are related by the equation of state,  $h_b = \mathcal{D} \text{sgn}(\phi) |\phi|^\delta F(t|\mathcal{B}/\phi|^{1/\beta})$ , where  $F(\hat{X}) = 1 + \hat{X}$  (in lowest order in  $\hat{X}$ ) is a universal (bulk) scaling func-

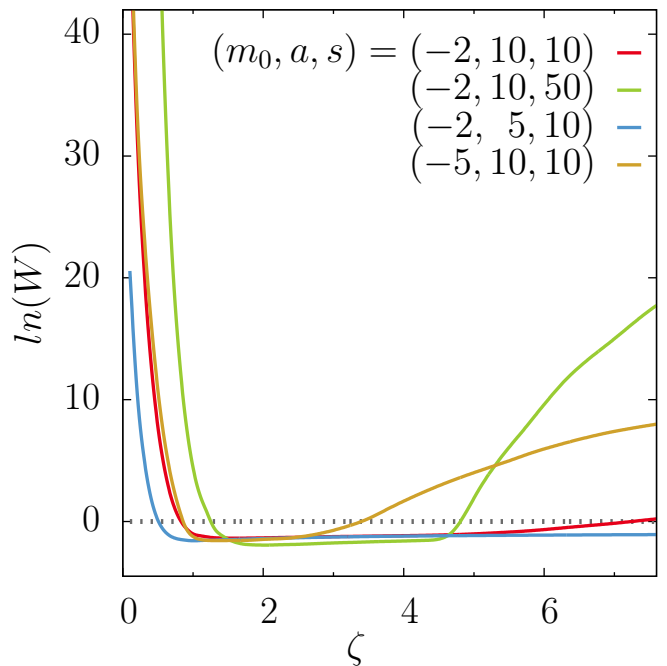


FIG. 3. Semi-logarithmic plot of the stability ratio  $W$  (Eq. (6)) for the typical experimental situation of varying the reduced temperature  $|t| \sim \zeta^{-1/\nu}$  at fixed composition  $(c_a - c_{a,c}^{(s)}) \sim m_0^{-1}$  (Eq. (8)). The steep decrease of  $\ln(W)$  towards negative values upon increasing  $\zeta$ , i.e., for  $t \rightarrow 0$ , suggests that coagulation sets in within a narrow temperature interval. The increase of  $W$  for large values of  $\zeta$  occurs for strongly repulsive contributions to the effective potential ( $a = 10$ , Eq. (5));  $s = \kappa R$ , where  $\kappa^{-1}$  is the range of the repulsive "background" potential and  $R$  is the radius of the colloids.

tion (see Appendix A in Ref. 2).  $\mathcal{B}$  and  $\mathcal{D}$  are non-universal amplitudes which depend on the definition of  $\phi$  such that on the coexistence curve the bulk OP follows  $\phi_b(t \rightarrow 0^-, h_b = 0) = \mathcal{B}|t|^\beta$  and that on the critical isotherm  $\phi_b(t = 0, h_b \rightarrow 0) = \text{sgn}(h_b) |h_b/\mathcal{D}|^{1/\delta}$ . For example, in binary liquid mixtures the order parameter  $\phi$  is proportional to the deviation of the concentration  $c_a$  of the component  $a$  from its critical value  $c_{a,c}^{(s)}$ ,  $\phi = \mathcal{A}(c_a - c_{a,c}^{(s)})$  (note that  $\mathcal{B}$  is proportional to  $\mathcal{A}$ ), which can be easily controlled by changing the mass or the volume fraction of one of the components of the mixture.

The steep decrease of  $W$  upon increasing  $\zeta \lesssim 1$  indicates that coagulation is expected to set in above the critical temperature (i.e.,  $W$  crossing the value 1 from above) within a rather narrow temperature interval. For the plots in Fig. 3 we have chosen parameter values which allow one to focus on the region of the onset of coagulation. As one can infer from the stability diagram (Fig. 2)  $a = 10$  corresponds to a relatively strong repulsion in the sense that for this value the range of values of  $\Sigma$  for which  $W < 1$  holds and thus coagulation occurs is rather

narrow. This implies that one finds  $W < 1$  only for intermediate values of  $\zeta$ . Such a case is represented by the red curve in Fig. 3 which corresponds to  $m_0 = -2$ ,  $a = 10$ , and  $s = 10$ . We find a clear increase of  $W$  for  $\zeta \gtrsim 4.5$ ; for larger  $\zeta$ ,  $W$  becomes even larger than 1. The effect of varying  $m_0$ ,  $a$ , or  $s$  relative to the red curve can be inferred from the brown, blue, and green curves, respectively. Since the height of the potential barrier is proportional to  $s$ , stability is significantly enhanced for larger values of  $s$  (see the green curve ( $s = 50$ ) in Fig. 3). The value of  $\zeta$ , for which  $\ln(W)$  turns from positive to negative (negative to positive) is larger (smaller) than the corresponding one for  $s = 10$ . For the composition corresponding to  $m_0 = -5$ , which is closer to the critical composition (see Eq. (8)), the region of values of  $\zeta$  for which  $W < 1$  is smaller than for  $m_0 = -2$  (see the brown curve in Fig. 3). Upon decreasing  $a$ , the value of  $\zeta$  for which  $\ln(W)$  changes from being positive to being negative becomes smaller (see the blue curve ( $a = 5$ )). For such small values of  $a$ ,  $\ln(W)$  remains negative upon increasing  $\zeta$  (also for values of the parameters  $m_0$  and  $s$  not shown in Fig. 3).

In summary, along the thermodynamic paths considered (and typically realized in experiments) the range of the attraction due to the CCFs grows steadily with increasing  $\zeta$ , but the amplitude of the CCFs is a non-monotonous function of  $\zeta$ . The CCF attains its maximal strength for an intermediate value of  $\zeta$ . Therefore, upon increasing  $\zeta$  the repulsive barrier in the effective pair potential is at first reduced; for sufficiently small values of  $a$  it can even disappear altogether. For even larger values of  $\zeta$ , the potential barrier may grow again (or emerge) because the amplitude of the CCF decreases again. This latter barrier is located at smaller values of  $D$  than the one which is present for small values of  $\zeta$ . The nonmonotonous dependence of the maximal strength of the CCF on temperature results in a nonmonotonous behavior of  $W = W(\zeta)$ . Although, as stated above, a repulsive barrier may emerge again, it is likely that aggregates, which have formed for intermediate values of  $\zeta$ , will not break up. This might be due to either specific microscopic interactions or due to the secondary minimum in the effective pair potential, which is still quite deep. Also in the case in which for all values of  $\zeta$  a repulsive barrier remains, coagulation can appear, due to a deep secondary minimum. This case will be discussed in Sect. VI.

## V. STRUCTURE

The bulk structure of a colloidal suspension is characterized by its radial distribution function  $g(r)$  which can be interpreted as the probability to find a colloidal particle a distance  $r$  apart from another particle fixed at the origin. The total correlation function (TCF)  $h(r)$  is related to the former one according to  $h(r) = g(r) - 1$ . The Ornstein-Zernicke equation expresses  $h(r)$  in terms

of the direct correlation function (DCF)  $c(r)$  and the number density  $\rho$ ,<sup>51,52</sup>

$$h(r) = c(r) + \rho \int h(r') c(|\mathbf{r} - \mathbf{r}'|) d^3\mathbf{r}', \quad (9)$$

or equivalently in Fourier space

$$\hat{h}(q) = \hat{c}(q) / (1 - \rho \hat{c}(q)), \quad (10)$$

with  $\hat{h}(\mathbf{q}) = \int e^{i\mathbf{q}\mathbf{r}} h(\mathbf{r}) d^d\mathbf{r}$ , analogously for  $\hat{c}(\mathbf{q})$ , and  $q = |\mathbf{q}|$ . In order to determine the two unknown functions  $c(r)$  and  $h(r)$  a second equation is required. This is the so-called closure equation which in its most general form is given by

$$h(r) + 1 = \exp\{-U(r) + h(r) - c(r) + b(r)\} \quad (11)$$

where  $b(r)$  is the so-called bridge function, which in general is not known. The most common approximations for the bridge function are the so-called Percus-Yevick approximation (PY),

$$b_{PY}(r) = \ln[h(r) - c(r) + 1] - h(r) + c(r), \quad (12)$$

and the so-called hypernetted-chain approximation (HNC),

$$b_{HNC}(r) = 0. \quad (13)$$

For practical reasons, in order to handle the hard core  $U(r < 2R) = \infty$ , it is useful to introduce the function

$$k(r) = h(r) - c(r). \quad (14)$$

In terms of  $k(r)$  the PY closure (Eq. (12)) can be written as

$$c_{PY}(r) = [\exp\{-U(r)\} - 1](k(r) + 1) \quad (15)$$

and the HNC closure (Eq. (13)) as

$$c_{HNC}(r) = \exp\{-U(r) + k(r)\} - k(r) - 1. \quad (16)$$

The correlation functions can be calculated iteratively.<sup>52,53</sup> For a given approximate  $c_i(r)$  one calculates the TCF  $h_i(r)$  according to Eq. (10). By using a closure, i.e., by choosing a bridge function, Eq. (11) renders a DCF  $c_{i+1}$  which typically differs from  $c_i$ . This procedure is continued until satisfactory convergence is achieved. The initial guess  $c_{i=1}(r)$  is guided by the shape of the direct interaction potential.

The applicability and reliability of this integral equation approach (IEA) is discussed in detail in Ref. 54. For comparison with Monte Carlo simulations in the case of a pair potential with attractive and repulsive parts see, e.g., Ref. 48, which discusses particles interacting with a pair potential containing attractive and repulsive Yukawa-like contributions  $\epsilon_i e^{-\kappa_i r}/r$ . The IEA is capable to reveal the rich phase behaviour of such systems.

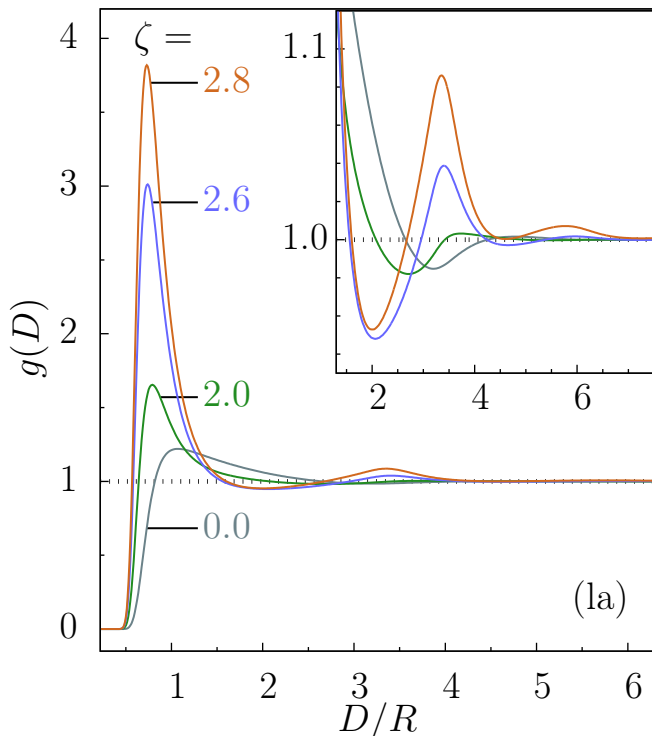


FIG. 4. The radial distribution function  $g(r)$  as obtained from the HNC closure (Eq. (13)) for four values of  $\zeta \sim |t|^{-\nu}$  and for a volume fraction  $\eta = 0.04$  of the colloids. The parameters of the corresponding effective potential (attractive at large distances (la), Eq. (5)) are  $a = 100$  for the strength of the repulsion,  $m_0 = -100$  for the reduced composition (Eq. (8)), and  $s = \kappa R = 10$ ;  $\kappa^{-1}$  is the range of the soft repulsion,  $R$  is the radius of the colloids, and  $D = r - 2R$  is the surface-to-surface distance. The sequence of curves corresponds to the generic isochoral thermodynamic path realized in experiments. For these values of the parameters, upon decreasing the reduced temperature  $t$ , i.e., increasing  $\zeta$ , a single attractive minimum develops in the effective potential. This increasing attraction due to the CCF leads to the enhancement of  $g(r)$  close to the surface of the colloid. This peak suggests that the formation of colloid dimers is favored. The inset provides an enlarged view of the vicinity of the second maximum of  $g(r)$ .

The structure factor

$$S(q) = 1 + \rho \hat{h}(q) = 1 / (1 - \rho \hat{c}(q)) \quad (17)$$

can be determined by scattering experiments. From sum rules it follows that the isothermal compressibility  $\chi_T$  is given by<sup>52</sup>

$$\lim_{q \rightarrow 0} S(q) = \rho k_B T \chi_T. \quad (18)$$

The system becomes unstable for  $\chi_T \rightarrow \infty$ , corresponding to the critical point and, within MFT, to the spinodals in the phase diagram (see, e.g., Ref. 55).

The diversity of possible shapes of the effective pair potential given in Eq. (5) (see Fig. 1) leads to a variety

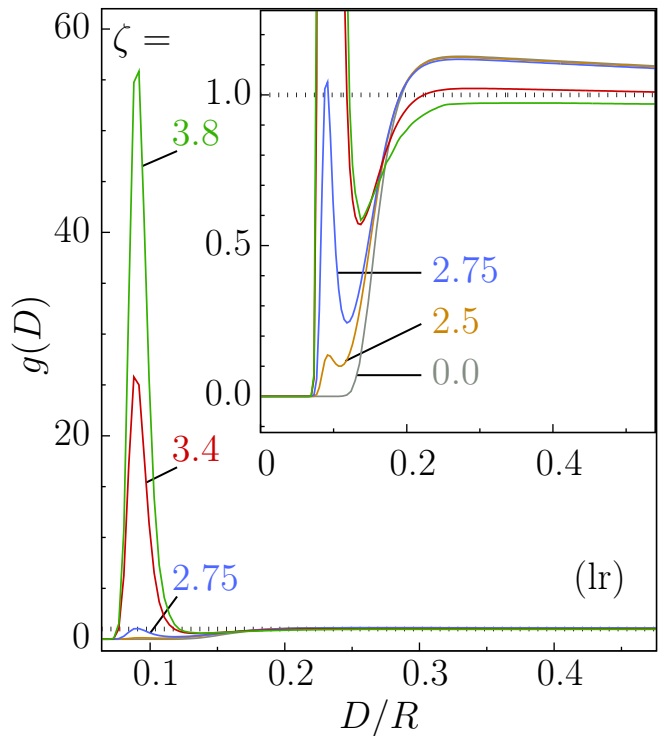


FIG. 5. The radial distribution function  $g(r)$  as obtained from the HNC closure (Eq. (13)) for various values of  $\zeta \sim |t|^{-\nu}$  and for a volume fraction  $\eta = 0.04$  of the colloids. The parameters of the corresponding effective potential (repulsive at large distances (lr), Eq. (5)) are  $a = 40$  for the strength of the repulsion,  $m_0 = -3$  for the reduced composition (Eq. (8)), and  $s = \kappa R = 50$ ;  $\kappa^{-1}$  is the range of the soft repulsion,  $R$  is the radius of the colloids, and  $D = r - 2R$  is the surface-to-surface distance. For these values of the parameters, upon decreasing the reduced temperature  $t$ , i.e., increasing  $\zeta$ , an attractive minimum develops in the effective potential at intermediate values of  $D$  while repulsion remains at small and large values of  $D$ . Due to this attraction a peak develops upon decreasing  $t$ . For a comparable potential well depth this peak is higher and narrower than in the case without a long-ranged repulsion (compare Fig. 4).

of radial distribution functions  $g(r)$  (see Figs. 4 and 5 in which the results for the HNC closure are shown; the results obtained using the Percus-Yevick closure are almost the same, differing mostly in that, for the same value of  $\zeta$ , the amplitude of the resulting  $g(r)$  is slightly smaller than the one within the HNC closure). For temperatures far away from the critical temperature of the solvent (i.e., for  $\zeta = \kappa \xi \ll 1$ ), the colloids are effectively hard spheres with an effective diameter  $\sigma > 2R$  due to the soft repulsive background contribution  $U_{rep}$ . Accordingly, for such values of  $\zeta$ ,  $g(r)$  has the corresponding characteristics of a fluid of hard spheres, such as the rather broad first peak for small values of  $D$ . Due to the emerging attractive CCFs, for increasing  $\zeta \sim |t|^{-\nu}$ , the radial distribution function  $g(r)$  is enhanced close to the surfaces of the colloids. This implies an enhanced short-ranged order.

In the case that the effective potential exhibits a repulsive barrier at small values of  $D$  and is attractive throughout large distances (denoted by (1a) in the following), we find that upon increasing  $\zeta$  the positions of the extrema of  $g(r)$  move towards smaller values of  $D$  (especially for intermediate values of  $\zeta$ ) and the value of  $g(r)$  at the maxima (minima) increases (decreases); the latter occurs mostly for larger values of  $\zeta$  (see Fig. 4).

In contrast, in the case of effective potentials which are repulsive at large distances (denoted by (1r) in the following), a new first peak at small values of  $D$  emerges and increases with increasing  $\zeta$  while the former first peak decreases and finally disappears (see the brown curve for  $\zeta = 2.5$  in Fig. 5 showing the emergence of a new peak at  $D/R \simeq 0.1$ ; the broad former first peak is located at larger distances  $D/R \simeq 0.25$ ). A similar trend is seen for the other extrema at larger  $D$ . However, since in that range of  $D$  the amplitude of  $g(r)$  is already quite small, the actual changes of the shape of  $g(r)$  cannot be described in such simple terms.

In homogeneous, i.e., not phase separated systems, the (newly emerged or shifted) first peak in  $g(r)$  can become significantly larger in the (1r) case than in the (1a) case (see Figs. 5 and 4, respectively, and note the different scales). The reason for this difference can be understood as follows. To a large extent the height of the first maximum in  $g(r)$  depends on the depth of the attraction well of the effective potential. Indeed, for comparable potential well depths the first peak in  $g(r)$  is only slightly larger in the (1r) case than in the (1a) case. However, for equally deep potential wells the overall attraction is stronger in the (1a) case due to the attraction throughout large distances (which gives rise to a larger compressibility  $\chi_T$  which is proportional to the integral of  $g(r) - 1$ ). Accordingly, the systems interacting via (1a) effective potentials can phase separate for shallower potential wells. Systems with potential well depths corresponding to large first peaks in  $g(r)$  (as the ones shown for the (1r) potentials in Fig. 5) and with a (1a) character would already be phase separated. In this sense, the repulsion occurring at larger values of  $D$  enhances the stability (w.r.t. phase separation) even of colloidal suspensions exhibiting large peaks in  $g(r)$  in homogeneous systems. In order to illustrate this point, we note that the compressibility corresponding to the blue curve ( $\zeta = 2.6$ ) in Fig. 4 turns out to be approximately the same as the one corresponding to the green curve ( $\zeta = 3.8$ ) in Fig. 5, although for the latter system the peak in  $g(r)$  is nearly 20 times larger.

## VI. COMPARISON WITH EXPERIMENTS

For dilute suspensions, the second virial coefficient<sup>52</sup>  $B_2$  provides information about the strength of the radii symmetric attraction between spherical particles:

$$B_2 = 2\pi \int_0^\infty (1 - \exp\{-U(r)\}) r^2 dr. \quad (19)$$

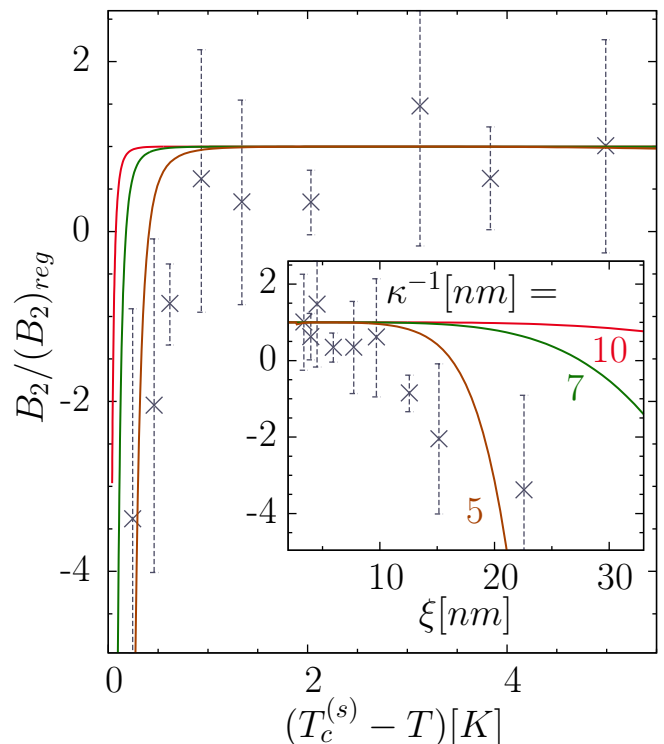


FIG. 6. The value of the second virial coefficient  $B_2$  (Eq. (19)) normalized by its value  $(B_2)_{reg}$  far away from  $T_c^{(s)}$  as function of the temperature deviation from the critical temperature  $T_c^{(s)}$  of the solvent and at its critical composition ( $\Sigma = 0$ ). The same data in the inset but as function of the correlation length  $\xi = \xi_0 |1 - T/T_c^{(s)}|^{-\nu}$  of the solvent. The experimental values (symbols) for latex particles immersed in the critical water-lutidine mixture are taken from Fig. 4 of Ref. 10(b). The lines correspond to the values obtained from the effective pair potential given in Eq. (5). The values of  $a$  and  $s$  were obtained by using Eq. (20) for  $A$  and the values  $\Upsilon = 5.7 \mu C/cm^2$  and  $2R = 555 nm$  as given in Ref. 10(b). We have considered various values of  $\kappa$  within the range reported in Ref. 10(b). We have adopted the values  $\xi_0 = 0.25 nm$  and  $T_c^{(s)} = 310 K$ . For the critical mass fraction  $\omega_{L,c} = 0.287$  of lutidine<sup>10(b)</sup> one obtains<sup>56</sup>  $\epsilon = 22.3$ . For further details see the main text.

Beyond the ideal gas contribution it determines the leading non-trivial term in the expansion of the pressure  $p(\rho)/(k_B T \rho) = 1 + B_2 \rho + \dots$  in terms of powers of the number density  $\rho$ .

In Ref. 10 the second virial coefficient  $B_2$  has been determined for latex particles immersed in a mixture of 2,6-lutidine and water by using light scattering. In Fig. 6, for the critical composition ( $\Sigma = 0$ ) we compare the variation of  $B_2$  upon approaching the critical temperature  $T_c^{(s)}$  for the effective pair potential in Eq. (5) with the experimental data given in Fig. 4 of Ref. 10(b). In order to be able to compare these data with  $U(r)$  given in Eq. (1) we have to specify the amplitude  $A$  of the repulsive contribution  $U_{rep}(r) = A \exp(-\kappa D)$ . This amplitude depends

on the surface charge density  $\Upsilon$  of the colloids:<sup>45</sup>

$$A = (\epsilon\epsilon_0)^{-1} \Upsilon^2 \kappa^{-2} R / (k_B T), \quad (20)$$

where  $\epsilon$  is the permittivity of the solvent relative to vacuum,  $\epsilon_0$  is the permittivity of the vacuum, and  $\kappa$  is the inverse Debye screening length. We have adopted the experimental values  $\Upsilon = 5.7 \mu\text{C}/\text{cm}^2$  and  $2R = 555 \text{nm}$  as given in Ref. 10(b). The relative permittivity  $\epsilon$  as function of the mass fraction  $\omega_L$  of lutidine can be obtained by using the Clausius-Mossotti relation<sup>23b,56</sup>. We have taken the values  $\xi_0 = 0.25 \text{nm}$  and  $T_c^{(s)} = 310 \text{K}$  as typical for water-lutidine mixtures (see, e.g., Ref. 32). In Ref. 10(b) no precise value of the Debye screening length  $\kappa^{-1}$  is given; it is stated that  $\kappa^{-1} \approx (7 \dots 10) \text{nm}$ . Therefore in Fig. 6 we show results for  $B_2$  calculated for several values of  $\kappa^{-1}[\text{nm}] = 5, 7, 10$ .

Within their analysis, for temperatures far away from  $T_c^{(s)}$  (i.e.,  $|T - T_c^{(s)}| \gtrsim 3 \text{K}$ ) the authors of Ref. 10(b) obtained values for  $B_2$  which would correspond to a system of hard spheres of a radius of  $4200 \text{nm}$ . These extremely large, unexpected values (they actually used particles of diameter  $555 \text{nm}$ ) cannot be easily explained by a soft, repulsive interaction<sup>10(b)</sup>. In order to circumvent this non-trivial effect, in Fig. 6 we plot  $B_2$  normalized by the corresponding values  $(B_2)_{reg}$  far away from  $T_c^{(s)}$ . For the normalization of the experimental data, we have used the mean values corresponding to the three largest temperature differences  $|T - T_c^{(s)}|$  which have been reported. For  $(B_2)_{reg}$  in the theoretical curves we have used the values as obtained by taking in Eq. (5) for  $x > 0$  only the soft, repulsive term into account (i.e., taking  $\zeta = \kappa\xi = 0$ ), so that  $(B_2)_{reg}/v_{HS} = 5.28, 6.00, 7.25$  for  $\kappa^{-1}[\text{nm}] = 5, 7, 10$ , respectively, where  $v_{HS} = (4\pi/3)R^3$  is the volume of the hard spheres.

Although we have adopted a rather simple form for the background repulsive potential, for  $\kappa^{-1} = 5 \text{nm}$  we obtain a fair agreement between the normalized experimental and theoretical values. Yet due to large error bars of the experimental data and large differences between not normalized experimental and theoretical values of  $B_2$  (the origin of which is unclear) we do not claim that this value of  $\kappa^{-1}$  is the actual experimental one. Rather we consider  $\kappa^{-1}$  in that case as an effective fitting parameter which accounts for differences between the experimentally realized and the model background potential in order to match the model with the experimental data. Furthermore, we have not checked the sensitivity of our results to uncertainties in the other parameters. Both from experiment and theory it is evident that the attraction close to the critical temperature increases significantly, resulting in a steep decrease of  $B_2$  towards large negative values.

In Ref. 10(b) the variation of  $B_2$  as function of  $|T - T_c^{(s)}|$  is reported also for a mass fraction  $\omega_L$  of lutidine larger than its critical value  $\omega_{L,c} \simeq 0.287$  (Fig. 7). (This value of  $\omega_{L,c} = 0.287$  is quoted in Ref. 10(b); it differs slightly from the value  $\omega_{L,c} = 0.286$  quoted in Ref. 3

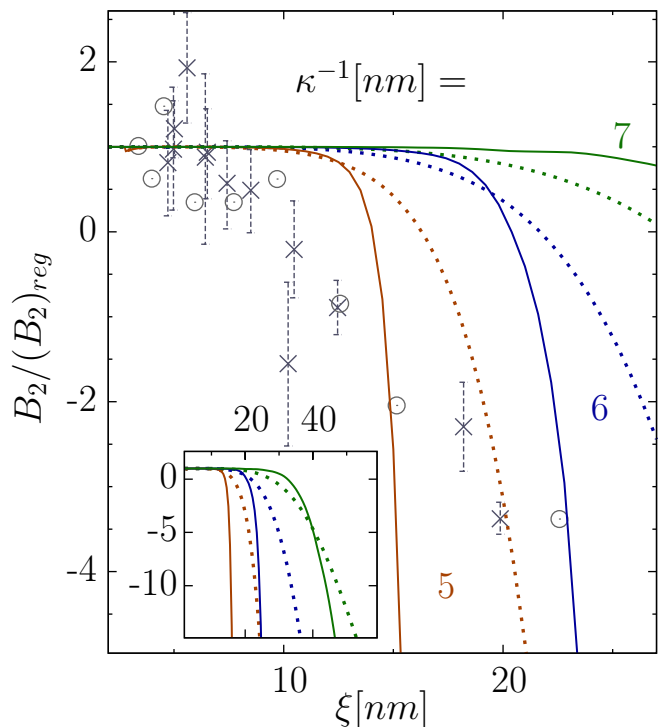


FIG. 7. The variation of the second virial coefficient  $B_2$  (Eq. (19)) upon approaching the critical temperature  $T_c^{(s)}$  for an off-critical composition of the binary solvent. The same data in the inset, but as function of the correlation length  $\xi = \xi_0 |1 - T/T_c^{(s)}|^{-\nu}$  of the solvent. The experimental values ( $\times$ ) are taken from Fig. 2 of Ref. 10(b) and the three theoretical curves are obtained by using the effective potential in Eq. (5). The values  $\kappa^{-1}[\text{nm}] = 7, 6$ , and  $5$  correspond to  $m_0 = -10.6, -13.5$ , and  $-18.0$ , respectively (Eq. (8)). For the lutidine mass fraction  $\omega_L = 0.35 \gtrsim \omega_{L,c}$  the solvent is poor in the component preferred by the colloids. Therefore the critical Casimir force is stronger than for the critical composition. Thus  $B_2$  can be expected to decrease more rapidly than for  $\omega_L = \omega_{L,c}$ . This is indeed the case for the theoretical curves. For the experimental data of Ref. 10(b) no dependence on  $\omega_L$  is seen; the dotted curves and the experimental data ( $\circ$ ) correspond to the critical composition as shown in Fig. 6.  $B_2$  is normalized in the same way as in Fig. 6. The order parameter amplitude used here is  $\mathcal{B}_\omega = 0.765$  (see Eq. (8), Ref. [73] in Ref. 2, and the text below Eq. (27) in Ref. 2). By making use of the Clausius-Mossotti relation<sup>23b,56</sup> we obtain  $\epsilon = 19.3$  (see Eq. (20)). The values of the other parameters are the same as in Fig. 6.

and as obtained from fitting the two-phase coexistence curve determined experimentally in Refs. 3 and 7 to the functional form  $|\omega_L - \omega_{L,c}| = \mathcal{B}_\omega |t|^\beta$  with  $\beta = 0.3256$ ; see Fig. 8. In other papers values are quoted within the range  $\omega_{L,c} = 0.28 \dots 0.29$ ; see, e.g., Refs. 3, 5, 6, and 32.) In general, for off-critical compositions the strength and the range of the critical Casimir force results from the interplay of the two bulk correlation lengths  $\xi \sim |t|^{-\nu}$  and  $\xi^{(h)} \sim |h_b|^{-\nu/(\beta\delta)}$  (see Eq. (1) and the discussion thereafter). For  $\omega_L = 0.35$  the binary solvent is poor

in the component preferred by the kind of colloids used (i.e., water). In such a case the interplay of  $\xi$  and  $\xi^{(h)}$  is rather complex due to the occurrence of capillary condensation which leads to bridging between two colloids. In particular, at the same temperature the CCF can become stronger upon moving away from the critical composition. But at off-critical compositions it is in general shorter ranged than at the critical composition. Moreover, at off-critical compositions the CCF emerges as function of temperature only closer to the critical temperature as compared with the corresponding thermodynamic path at the critical composition. In Fig. 7 we compare the reduced experimental data for  $B_2$  corresponding to the mass fraction  $\omega_L = 0.35 > \omega_{L,c} = 0.287$  with the theoretical curves obtained within our effective model; for  $\omega_L = 0.35$  one has  $(B_2)_{reg}/v_{HS} = 5.30, 5.65, 6.03$  for  $\kappa^{-1}[nm] = 5, 6, 7$ , respectively. As can be inferred from Fig. 7 for  $\kappa^{-1} = 5nm$  the total attraction (within our effective model), in terms of  $B_2$ , is stronger for  $\omega_L = 0.35$  than for the critical composition  $\omega_{L,c}$ , i.e., for the same value of  $\xi$ ,  $B_2$  is more negative. For the theoretical curve corresponding to  $\kappa^{-1} = 7nm$  the aforementioned interplay of  $\xi$  and  $\xi^{(h)}$  manifests itself more clearly. For the off-critical composition the attraction due to the CCFs sets in only for larger values of  $\xi$  but becomes more rapidly stronger with increasing  $\xi$  so that, for large values of  $\xi$ ,  $B_2$  is more negative for  $\omega_L = 0.35$  than for  $\omega_{L,c}$ . At the critical composition,  $B_2$  starts to decrease (due to the attractive CCFs) already for smaller values of  $\xi$  than for  $\omega_L = 0.35$ .

For the experimental data (within the large error bars and the reported temperature range) no dependence of the value of  $B_2$  as function of  $|T - T_c^{(s)}|$  on the composition is observed. (Reference 10(b) provides the values of  $B_2$  as function of  $|T - T_{cx}^{(s)}|$  but lacks an absolute value for the coexistence temperature  $T_{cx}^{(s)}$ ;  $T_{cx}^{(s)}$  is the temperature at which the solvent undergoes a first-order phase segregation for  $\omega_L = 0.35 \neq \omega_{L,c}$ ; see Fig. 1(a) in Ref. 2. We take  $T_{cx}^{(s)} - T_c^{(s)} = 0.145K$  as obtained<sup>2</sup> from  $|\omega_L - \omega_{L,c}| = \mathcal{B}_\omega |t|^\beta$  with  $\mathcal{B}_\omega = 0.765$ .) This finding is in contrast to the behavior of the measured effective particle-wall interaction potentials of Ref. 57, for which a dependence on the composition of the water-lutidine mixture has been observed. At present it remains unclear whether the dependence of  $B_2$  on  $\omega_L$  could not be resolved experimentally or whether the data from these experiments happen to lie in that crossover regime in which the curves  $B_2(T_c^{(s)} - T)$  happen to be close to each other for the critical and the off-critical mixture (see the inset in Fig. 7).

For the same system the authors of Ref. 10(b) used for the measurement of  $B_2$ , in Ref. 7(b) the aggregation phenomena of immersed colloids have been studied. We have used the corresponding given experimental values of the parameters, and especially Eq. (20) for the repulsion strength parameter  $A$ , in order to investigate these state

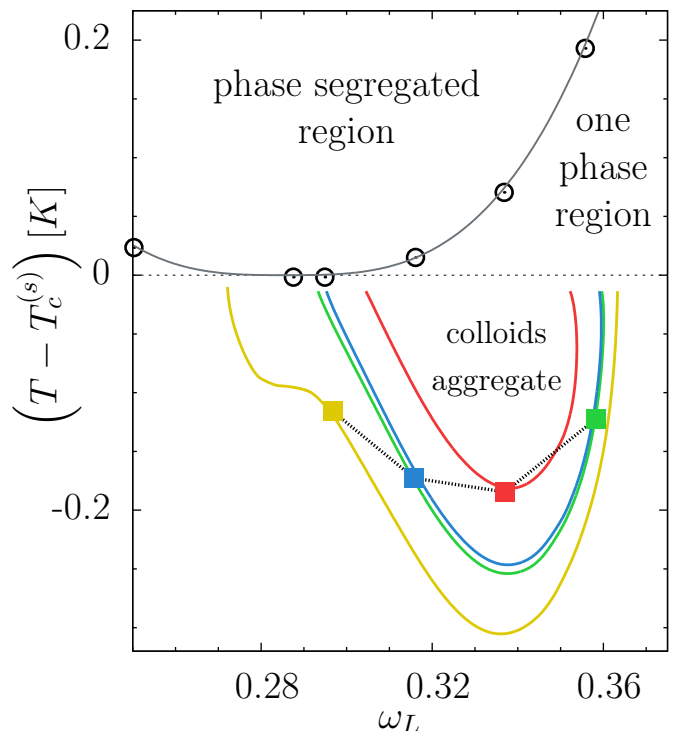


FIG. 8. Comparison of the values of  $B_2$  (Eq. (19)) at the thermodynamic state points of the solvent for which immersed colloids aggregate. The four experimentally obtained state points (squares; the straight black dotted lines in between are a guide to the eye) are taken from Fig. 1 (middle) of Ref. 7(b)). The isolines of constant  $B_2$  (full colored lines), each belonging to one of the state points (squares), are calculated within our model (Eq. (5)). Each  $B_2$ -isoline can capture some qualitative trends of the possible shape of the line of the onset of aggregation, but they cannot serve as quantitative indicators for the onset of aggregation. For further details see the main text. In order to obtain the theoretical values of  $B_2$  we have taken  $\xi_0 = 0.25nm$ ,  $\kappa^{-1} = 6nm$ ,  $T_c^{(s)} = 307K$ , and  $\omega_{L,c} = 0.286$  and we have used the experimentally given values  $2R = 378nm$  and  $\Upsilon = 3.85\mu C/cm^2$ . The repulsion strength  $A$  is obtained from Eq. (20) with  $\epsilon$  depending, according to the Clausius-Mossotti relation<sup>23b,56</sup>, on the mass fraction  $\omega_L$  of lutidine. The experimentally determined coexistence points (circles) on the binodal of phase segregation with a lower critical point agree well with the relation  $|\omega_L - \omega_{L,c}| = \mathcal{B}_\omega |t|^\beta$ , where  $\beta = 0.3256$  and  $\mathcal{B}_\omega = 0.765$  (gray line); in accordance with a lower critical point the reduced temperature is  $t = (T_c^{(s)} - T)/T_c^{(s)}$ .

points within our model.

First, it is worthwhile to mention that for the parameters corresponding to these experiments, the repulsive barrier for small values of  $x = \kappa D$  is of the order of tens of  $k_B T$ . Therefore, it seems that the observed aggregation is due to the very deep secondary minimum emerging at a certain distance  $D_{min}$ . This is a different mechanism than the one discussed in Sect. IV, where the aggregation due to the disappearance of the repulsive barrier at short distances  $D$  has been considered.

While in the latter case the colloids would stick together with their surfaces at contact, in the former case they are close but not at contact. With  $\kappa D_{min} \approx 1$  and  $s = \kappa R \approx 10 \dots 100$ , from the effective potential given in Eq. (5) it follows that the colloids are a surface-to-surface distance  $D/R \approx 10^{-1} \dots 10^{-2}$  apart. In Ref. 7(b) the mean surface-to-surface distance has not been estimated, but in experiments performed for a similar system (see Ref. 6) it has been found that in the flocculated and sedimented aggregates the average interparticle distance is about three times the mean radius of the polydisperse colloids. This is in the stark contrast with our theoretical estimates. Other experimental reports do not specify the average interparticle distance occurring in the aggregates. In Ref. 14 it is stated, that the sediment is less dense than expected for a tight packing of spheres and in Ref. 17 the aggregates are characterized as being compact, not fractal. The authors of Ref. 13 argue that for their system the aggregates are indeed crystalline. The possibility, that the flocculated colloidal particles form a bona fide, thermodynamically stable, liquid-like or crystalline phase cannot be addressed within the effective, one-component approach used here, because within this approach the reliable prediction of the occurrence of a phase transition can be made only if the colloidal number density is sufficiently large (see Ref. 2, especially, Subsect. III B 3), whereas in the experiments referred to above the packing fraction is as small as  $\eta \approx 10^{-6} \dots 10^{-3}$ .

Next, we address the issue whether a relation can be established which connects the onset of the reversible aggregation to a threshold of a specific quantity which is both theoretically and experimentally accessible. To do so we follow Ref. 10 and analyze whether the values of  $B_2$  corresponding to thermodynamic state points of the solvent, at which the aggregation of colloids sets in, are similar. For such state points, as determined experimentally and reported in Fig. 1 (middle) of Ref. 7(b), we have calculated the corresponding values of  $B_2$  within our model for four values of  $\omega_L$  yielding<sup>58</sup>  $B_2 / (\frac{4\pi}{3} R^3) = -7400$  (red square),  $-560$  (blue),  $-200$  (green), and  $-76.0$  (yellow) (Fig. 8). In Fig. 8 the isolines of constant  $B_2$  for these values of  $B_2$  are shown (using the same color code). Clearly the four curves do not coincide to form a single curve with the four squares on it which would support the hypothesis that aggregation sets in at a threshold of value of  $B_2$ . However, one has to keep in mind that the CCFs strongly depend on the temperature. This dependence is amplified within the resulting value of  $B_2$  due to its exponential dependence on the potential. Therefore the value of  $B_2$  may vary significantly even within a narrow temperature interval (compare Figs. 6 and 7). Moreover, small uncertainties in the measured temperature, at which the aggregation sets in, result in a large variation of  $B_2$ . Each  $B_2$ -isoline reproduces some of the qualitative trends of the experimental data points for aggregation onset, but there is no satisfactory quantitative agreement. Either the isoline is too narrow (see the red

curve which cannot capture any of the yellow, blue, or green squares) or the isoline extends to too large values of  $|T - T_c^{(s)}|$  (see, e.g., the yellow curve which misses the blue, red, and green squares). Besides the possibility that  $B_2$  is indeed not the same at the various state points at which coagulation sets in, there are further reasons which could explain this disagreement. One reason could be the simplified choice for the background potential which we have used. Furthermore, there are several experimental parameters for which we could use only estimates. Within their analysis, the authors of Ref. 7(a) conclude that for calculating the electrostatic potentials one should not use the bare surface charge density as given by the manufacturer. Rather, the dissociation of the colloidal surface in the solvent has to be taken into account. In our analysis we took the nominal value for the surface charge due to the lack of more detailed data. The authors of Ref. 9 point this out, too, and reveal the role of impurities as another important factor. They determined the aggregation line in “fresh” mixtures and in the same mixture but one or several days later. While the aggregation phenomenon as such was reproducible, the values of the thermodynamic variables of the solvent at which the aggregation sets in varied strongly within one and the same sample.

In the same reference, a dependence of the aggregation line on the volume fraction  $\eta$  of colloids is observed, whereas in Ref. 13 it is stated that the shape of the region in thermodynamic space where aggregates are forming does neither depend on the colloidal concentration nor on the colloidal radius. In Ref. 7(b) a dependence of the time scale of the aggregation process on  $\eta$  is reported. Our analysis does not capture such a dependence.

In conclusion, our results suggest that the critical Casimir force plays an important role in order to explain the aggregation phenomenon in this region of the phase diagram of the solvent. Yet, in order to be able to determine all relevant mechanisms and forces and in order to obtain quantitative agreement between the experiments and the theoretical results, for both further efforts are needed to provide more precise values of the relevant quantities.

Finally, in Fig. 8 experimental data for the binodal of the water-lutidine mixture are shown, which nicely agree with the functional form  $\omega_L - \omega_{L,c} = \pm \mathcal{B}_\omega |t|^\beta$  (gray line), where  $\beta = 0.3256$  and  $\mathcal{B}_\omega = 0.765$ . This shows that our description, which is symmetric w.r.t.  $\omega_L = \omega_{L,c}$ , is sufficient for the phase space region of interest here.

## VII. SUMMARY

We have studied aggregation phenomena of monodisperse colloidal suspensions with near-critical solvents. In such solvents, driven by the diverging bulk correlation length  $\xi \left( t = \left( T_c^{(s)} - T \right) / T_c^{(s)} \rightarrow 0^\pm \right) = \xi_0^\pm |t|^{-\nu}$ , so-called critical Casimir forces act on the colloidal par-

ticles, in addition to regular background forces. In order to obtain our results, we have adopted a description in terms of an effective one-component system. Within this approach the presence of the solvent is taken into account via contributions to the effective pair potential of the colloids. We have considered an effective pair potential for the colloids (with radius  $R$ ) which consists of the critical Casimir contribution plus a regular background potential. For the latter we have employed a generic, softly repulsive contribution with strength  $A$  and acting on a length scale  $\kappa^{-1}$ . We have focused on dilute suspensions with low colloidal number densities  $\rho$ , for which the approximation of pairwise additive critical Casimir forces (CCFs) is valid. In addition, we have applied the Derjaguin approximation (Eq. (2)), within which the pair potential between two spheres can be expressed in terms of the scaling function of the CCF in a slab. In order to obtain access to the dependence of the universal scaling function for the CCF on the scaling variable  $\Sigma$  associated with the bulk ordering field  $h_b$  in spatial dimension  $d = 3$  we have employed an approximation based on a combination of both Monte Carlo simulation data and of mean-field theory results (Eq. (3)). The resulting effective pair potential is given in Eq. (5) and various examples are plotted in Fig. 1. On this basis we have obtained the following main results:

1. We have calculated the stability ratio  $W \sim t_{pair}/t_{diff}$  (Eqs. (6) and (7)), which is a measure of the stability of a colloidal suspension. The time scales  $t_{pair}$  and  $t_{diff}$  are related to the pairing of two colloids and to the diffusion of a single particle, respectively. Rapid coagulation is expected to set in for  $W < 1$ . In Fig. 2 the contour lines  $W = 1$  are shown for various values of  $\zeta = \kappa\xi \sim |t|^{-\nu}$  and  $s = \kappa R$  in the space spanned by the parameter  $a = A/s$  and by the scaling variable  $\Sigma$ . For the case of a binary liquid mixture  $\Sigma$  is related to the difference of the chemical potentials of the two species. This shows that the CCF can lead to rapid coagulation. The coagulation region extends to larger values of  $a$  for  $\Sigma \lesssim 0$  because the CCFs are stronger for compositions of the solvent slightly poor in the component preferred by the colloids.
2. The variation of  $W$  with temperature at a fixed solvent composition, as it is typically realized in experiments, is shown in Fig. 3. We find that  $W$  rapidly decreases to  $W < 1$  upon approaching the critical temperature via the disordered phase. This implies, that the aggregation should set in within a narrow temperature interval.
3. Concerning the structure of the colloidal suspension, we have solved numerically the Ornstein-Zernicke equation (Eq. (9)) using the Percus-Yevick and the hypernetted-chain closure (Eqs. (15) and (16), respectively). In Figs. 4 and 5 we show the radial distribution function  $g(r)$  for two different

parameter sets  $(a, s, m_0)$  and various values of  $\zeta$ , where  $m_0^{-1} \sim c_a - c_{a,c}^{(s)}$  is related to the composition of the solvent (Eq. (8)). Close to the surface of a colloidal particle ( $r \gtrsim 2R$ ) a peak develops for increasing values of  $\zeta$ , reflecting the increasing attraction due to the CCF. This indicates the presence of a pronounced short-ranged order and that the formation of colloidal dimers is favored.

4. In Figs. 6 and 7, for the critical and for an off-critical composition, respectively, we compare the variation of the second virial coefficient  $B_2$  (Eq. (19)) upon increasing  $\xi = \xi_0 |t|^{-\nu}$ , as obtained within our model, with experimental data<sup>10(b)</sup>. For both, the theoretical results and the experimental data, for increasing  $\xi$  the virial coefficient  $B_2$  decreases towards large negative values. Due to extremely large experimental values of  $|B_2|$  also far away from  $T_c^{(s)}$ , the origin of which is not clear, the quality of the quantitative comparison is limited. For the off-critical composition, the CCF can become stronger than at the critical composition but it has in general a shorter range and occurs closer to the critical temperature of the solvent. Therefore, for the same value of  $\xi$ , the total attraction due to the CCFs can either be smaller or larger for an off-critical composition compared with the critical one. Accordingly, as can be seen in Fig. 7,  $B_2$  can be less or more negative, respectively. For the experimental data of Ref. 10(b) there is no visible dependence on the composition of the solvent, which could be due to this crossover behavior.
5. We have addressed the issue whether a relationship can be established between the onset of aggregation and a specific quantity which is accessible both theoretically and experimentally. To this end, within our model we have calculated  $B_2$  at state points for which in experiments aggregation sets in. The corresponding  $B_2$ -isolines capture qualitatively the main trends of the aggregation line, but no satisfactory quantitative agreement has been achieved (see Fig. 8). We have discussed various possible explanations for this discrepancy.

To conclude, our results show that CCFs, which can be easily controlled by temperature  $T$  and the strength and range of which can be varied by changing the bulk ordering field  $h_b$ , can lead to aggregation in colloidal suspensions with near-critical solvents. Within the approach of using an effective potential, we have identified the ranges of values for the background repulsive potential and the values of the scaling variables associated with the critical solvent, for which the colloids aggregate.

## ACKNOWLEDGMENTS

We acknowledge S. Buzzaccaro and R. Piazza for informing us about their experimental results in Ref. 16 before publication. We thank R. Evans for his generous interest in our work and the stimulating and enlightening discussions we enjoyed to have with him.

- <sup>1</sup>M. E. Fisher and P. G. de Gennes, *C. R. Acad. Sci., Paris, Ser. B* **287**, 207 (1978).
- <sup>2</sup>T. F. Mohry, A. Maciołek, and S. Dietrich, preceding paper, preprint, arXiv:1201.5540.
- <sup>3</sup>D. Beysens and D. Estève, *Phys. Rev. Lett.* **54**, 2123 (1985).
- <sup>4</sup>J. D. Cox, and E. F. G. Herington, *Trans. Faraday Soc.* **52**, 926 (1956).
- <sup>5</sup>Y. Jayalakshmi, J. S. Van Duijneveldt, and D. Beysens, *J. Chem. Phys.* **100**, 604 (1994).
- <sup>6</sup>V. Gurfein, D. Beysens, and F. Perrot, *Phys. Rev. A* **40**, 2543 (1989).
- <sup>7</sup>(a) P. D. Gallagher and J. V. Maher, *Phys. Rev. A* **46**, 2012 (1992); (b) P. D. Gallagher, M. L. Kurnaz, and J. V. Maher, *Phys. Rev. A* **46**, 7750 (1992).
- <sup>8</sup>M. L. Broide, Y. Garrabos, and D. Beysens, *Phys. Rev. E* **47**, 3768 (1993).
- <sup>9</sup>T. Narayanan, A. Kumar, E. S. R. Gopal, D. Beysens, P. Guenoun, and G. Zalczer, *Phys. Rev. E* **48**, 1989 (1993).
- <sup>10</sup>(a) M. L. Kurnaz and J. V. Maher, *Phys. Rev. E* **51**, 5916 (1995); (b) M. L. Kurnaz and J. V. Maher, *Phys. Rev. E* **55**, 572 (1997).
- <sup>11</sup>Y. Jayalakshmi and E. W. Kaler, *Phys. Rev. Lett.* **78**, 1379 (1997).
- <sup>12</sup>S. R. Kline and E. W. Kaler, *Langmuir* **10**, 412 (1994).
- <sup>13</sup>R. D. Koehler and E. W. Kaler, *Langmuir* **13**, 2463 (1997).
- <sup>14</sup>(a) H. Grill and D. Woermann, *Ber. Bunsenges. Phys. Chem.* **101**, 814 (1997); (b) B. Rathke, H. Grill, and D. Woermann, *J. Colloid Interface Sci.* **192**, 334 (1997).
- <sup>15</sup>(a) D. Bonn, J. Otwinowski, S. Sacanna, H. Guo, G. Wegdam, and P. Schall, *Phys. Rev. Lett.* **103**, 156101 (2009); (b) A. Gambassi and S. Dietrich, *Phys. Rev. Lett.* **105**, 059601 (2010); (c) D. Bonn, G. Wegdam, and P. Schall, *Phys. Rev. Lett.* **105**, 059602 (2010).
- <sup>16</sup>(a) S. Buzzaccaro, J. Colombo, A. Parola, and R. Piazza, *Phys. Rev. Lett.* **105**, 198301 (2010); (b) R. Piazza, S. Buzzaccaro, A. Parola, and J. Colombo, *J. Phys.: Condens. Matter* **23**, 194114 (2011).
- <sup>17</sup>(a) D. Beysens, J.-M. Petit, T. Narayanan, A. Kumar, and M. L. Broide, *Ber. Bunsenges. Phys. Chem.* **98**, 382 (1994); (b) D. Beysens and T. Narayanan, *J. Stat. Phys.* **95**, 997 (1999).
- <sup>18</sup>C. Bauer, T. Bieker, and S. Dietrich, *Phys. Rev. E* **62**, 5324 (2000); and references therein.
- <sup>19</sup>F. Schlesener, A. Hanke, and S. Dietrich, *J. Stat. Phys.* **110**, 981 (2003).
- <sup>20</sup>T. J. Sluckin, *Phys. Rev. A* **41**, 960 (1990).
- <sup>21</sup>R. R. Netz, *Phys. Rev. Lett.* **76**, 3646 (1996).
- <sup>22</sup>H. Löwen, *Phys. Rev. Lett.* **74**, 1028 (1995).
- <sup>23</sup>(a) B. M. Law, J.-M. Petit, and D. Beysens, *Phys. Rev. E* **57**, 5782 (1998); (b) J.-M. Petit, B. M. Law, and D. Beysens, *J. Colloid Interface Sci.* **202**, 441 (1998).
- <sup>24</sup>R. Okamoto and A. Onuki, *Phys. Rev. E* **84**, 051401 (2011).
- <sup>25</sup>(a) M. N. Barber in *Phase Transitions and Critical Phenomena*, edited by C. Domb and J. L. Lebowitz (Academic, New York, 1983), Vol. 8, p. 149; (b) V. Privman, in *Finite Size Scaling and Numerical Simulation of Statistical Systems*, edited by V. Privman (World Scientific, Singapore, 1990), p. 1.
- <sup>26</sup>H. W. Diehl in *Phase Transitions and Critical Phenomena*, edited by C. Domb and J. L. Lebowitz (Academic, New York, 1986), Vol. 10, p. 76.
- <sup>27</sup>M. Krech, *Casimir Effect in Critical Systems* (World Scientific, Singapore, 1994); *J. Phys.: Condens. Matter* **11**, R391 (1999).
- <sup>28</sup>G. Brankov, N. S. Tonchev, and D. M. Danchev, *Theory of Critical Phenomena in Finite-Size Systems* (World Scientific, Singapore, 2000).
- <sup>29</sup>A. Gambassi, *J. Phys.: Conf. Ser.* **161**, 012037 (2009).
- <sup>30</sup>A. Hanke, F. Schlesener, E. Eisenriegler, and S. Dietrich, *Phys. Rev. Lett.* **81**, 1885 (1998).
- <sup>31</sup>B. Derjaguin, *Kolloid Zeitschrift* **69**, 155 (1934).
- <sup>32</sup>A. Gambassi, A. Maciołek, C. Hertlein, U. Nellen, L. Helden, C. Bechinger, and S. Dietrich, *Phys. Rev. E* **80**, 061143 (2009).
- <sup>33</sup>O. Vasilyev, A. Gambassi, A. Maciołek, and S. Dietrich, *EPL* **80**, 60009 (2007); O. Vasilyev, A. Gambassi, A. Maciołek, and S. Dietrich, *Phys. Rev. E* **79**, 041142 (2009).
- <sup>34</sup>M. Hasenbusch, *Phys. Rev. B* **82**, 104425 (2010).
- <sup>35</sup>M. Hasenbusch, *Phys. Rev. B* **83**, 134425 (2011).
- <sup>36</sup>O. Vasilyev, A. Maciołek, and S. Dietrich, *Phys. Rev. E* **84**, 041605 (2011).
- <sup>37</sup>M. Krech, *Phys. Rev. E* **56**, 1642 (1997).
- <sup>38</sup>(a) Z. Borjan and P. J. Upton, *Phys. Rev. Lett.* **81**, 4911 (1998); (b) *ibid* **101**, 125702 (2008).
- <sup>39</sup>(a) M. E. Fisher and P. J. Upton, *Phys. Rev. Lett.* **65**, 2402 (1992); (b) *ibid* **65**, 3405 (1992).
- <sup>40</sup>C. Hertlein, L. Helden, A. Gambassi, S. Dietrich, and C. Bechinger, *Nature* **451**, 172 (2008).
- <sup>41</sup>U. Nellen, L. Helden, and C. Bechinger, *EPL* **88**, 26001 (2009).
- <sup>42</sup>M. Fukuto, Y. F. Yano, and P. S. Pershan, *Phys. Rev. Lett.* **94**, 135702 (2005).
- <sup>43</sup>T. F. Mohry, A. Maciołek, and S. Dietrich, unpublished.
- <sup>44</sup>J.-L. Barrat and J.-P. Hansen, *Basic concepts for simple and complex liquids* (Cambridge University Press, Cambridge, 2003).
- <sup>45</sup>W. B. Russel, D. A. Saville, W. R. Schowalter, *Colloidal Dispersions* (Cambridge University Press, Cambridge, 1989).
- <sup>46</sup>A. Pelissetto and E. Vicari, *Phys. Rep.* **368**, 549 (2002).
- <sup>47</sup>E. Eisenriegler and M. Stapper, *Phys. Rev. B* **50**, 10009 (1994).
- <sup>48</sup>A. J. Archer, and N. B. Wilding, *Phys. Rev. E* **76**, 031501 (2007).
- <sup>49</sup>A. Ciach, *Phys. Rev. E* **78**, 061505 (2008).
- <sup>50</sup>N. Fuchs, *Z. Phys. Chem.* **171**, 199 (1934).
- <sup>51</sup>L. S. Ornstein, and F. Zernike, *Proc. Acad. Sci. Amsterdam* **17**, 793 (1914).
- <sup>52</sup>J. P. Hansen and I. R. McDonald, *Theory of Simple Liquids* (Academic, London, 1986).
- <sup>53</sup>M. J. Gillan, *Mol. Phys.* **38**, 1781 (1979).
- <sup>54</sup>C. Caccamo, *Phys. Rep.* **274**, 1 (1996).
- <sup>55</sup>K. Binder, C. Billotet and P. Miñold, *Z. Phys. B* **30**, 183 (1978).
- <sup>56</sup>The Clausius-Mossotti relation<sup>23b</sup> expresses the relative (to vacuum) permittivity  $\epsilon$  of a binary liquid mixture in terms of the volume fraction  $\Phi_a$  of the component  $a$  and the relative permittivities  $\epsilon_{a,b}$  of the two components  $a$  and  $b$ :  $f(\epsilon) = \Omega(\Phi_a f(\epsilon_a) + (1 - \Phi_a) f(\epsilon_b))$ , where  $f(\epsilon) = (\epsilon - 1)/(\epsilon + 2)$  and  $\Omega$  is the fractional volume change upon mixing for which we adopt<sup>23b</sup>  $\Omega = 1$ . The volume fraction  $\Phi_a$  expressed in terms of the mass fraction  $\omega_a$  is  $\Phi_a = \omega_a \rho_{m,b} / [(1 - \omega_a) \rho_{m,a} + \omega_a \rho_{m,b}]$ , where  $\rho_{m,a}$  ( $\rho_{m,b}$ ) is the mass density of component  $a$  ( $b$ ); this expression follows from the relation  $\omega_a = \rho_{m,a} \Phi_a / (\rho_{m,a} \Phi_a + \rho_{m,b} \Phi_b)$  given in Ref. [73] in Ref. 2. For the mass density and the relative permittivity of pure lutidine (of pure water) we adopt the values<sup>5</sup>  $\rho_{m,L} = 0.911 \text{ g/cm}^3$  ( $\rho_{m,W} = 0.995 \text{ g/cm}^3$ ) and<sup>23b</sup>  $\epsilon_L = 7.33$  ( $\epsilon_W = 81$ ), respectively.
- <sup>57</sup>U. Nellen, doctoral thesis, University of Stuttgart (2011).
- <sup>58</sup>Often the ratio  $B_2^* = B_2/B_2^{(HS)} = \frac{1}{4} \left(\frac{2R}{\sigma}\right)^3 B_2 / \left(\frac{4\pi}{3} R^3\right)$  is used as a reduced second virial coefficient, where  $B_2^{(HS)} = (2\pi/3) \sigma^3$  is the second virial coefficient for a reference hard-sphere (HS) system with an effective HS diameter  $\sigma$ . Because the value of  $\sigma$  accounts for both the HS core and the short-ranged, softly repulsive contribution to the pair potential one has  $\sigma > 2R$ . A common way<sup>52</sup> to define  $\sigma$  (for potentials which cross over from being softly repulsive at small distances and being attractive for larger ones) is  $\sigma = \int_0^{r_0} (1 - \exp\{-U(r)\}) dr$  where  $U(r = r_0) = 0$  (see also Eq. (16) in Ref. 2). Accordingly, the value of  $\sigma$  varies explicitly with temperature and depends on the values of the

parameters in the potential  $U(r)$ . For the cases considered here  $\sigma/(2R)$  varies within the range 1.03...1.05.